

Analytical Methods

Accepted Manuscript



This is an *Accepted Manuscript*, which has been through the Royal Society of Chemistry peer review process and has been accepted for publication.

Accepted Manuscripts are published online shortly after acceptance, before technical editing, formatting and proof reading. Using this free service, authors can make their results available to the community, in citable form, before we publish the edited article. We will replace this *Accepted Manuscript* with the edited and formatted *Advance Article* as soon as it is available.

You can find more information about *Accepted Manuscripts* in the [Information for Authors](#).

Please note that technical editing may introduce minor changes to the text and/or graphics, which may alter content. The journal's standard [Terms & Conditions](#) and the [Ethical guidelines](#) still apply. In no event shall the Royal Society of Chemistry be held responsible for any errors or omissions in this *Accepted Manuscript* or any consequences arising from the use of any information it contains.

Synthesis, cytotoxicity and bioimaging of novel Hg²⁺ selective fluorogenic chemosensor

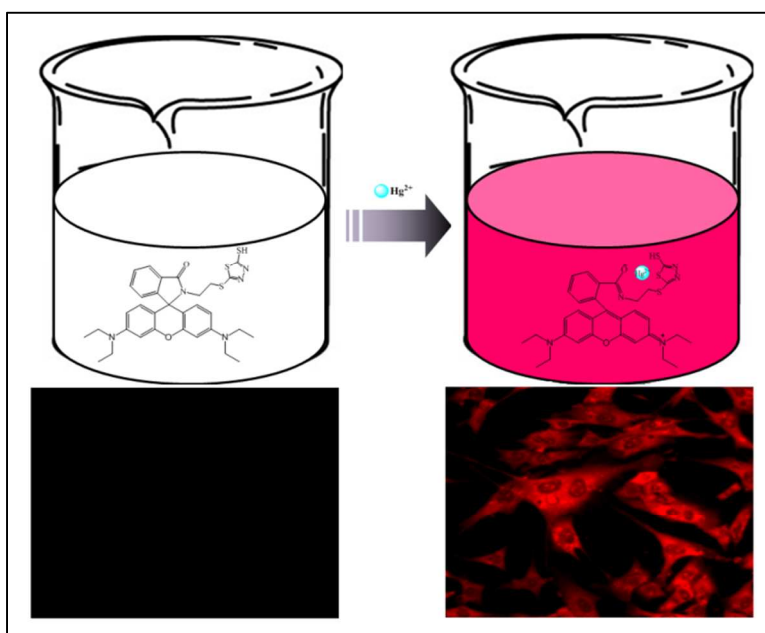
Muhammad Saleem^a, Razack Abdullah^a, Anser Ali^b, Bong Joo Park^b, Eun Ha Choi^b, In Seok Hong^a, Ki Hwan Lee^{a,*}

^aDepartment of Chemistry, Kongju National University, Gongju, Chungnam 314-701, Republic of Korea

^bDepartment of Plasma Bioscience and display, Kwangwoon University, 20 Kwangwoon-gil, Nowon-gu, Seoul 139-701, Republic of Korea

*corresponding author: Fax: +82-41-856-8613; E-mail address: khlee@kongju.ac.kr

Graphical abstract:



Synthesis, cytotoxicity and bioimaging of novel Hg²⁺ selective fluorogenic chemosensor

Cite this: DOI: 10.1039/x0xx00000x

Muhammad Saleem^a, Razack Abdullah^a, Anser Ali^b, Bong Joo Park^b, Eun Ha Choi^b, In Seok Hong^a, Ki Hwan Lee^{a,*}

Received 00th February 2014,
Accepted 00th -----

Abstract

DOI: 10.1039/x0xx00000x

www.rsc.org/

A rhodamine B derivative **2** with terminal mercapto thiazole moiety was successfully synthesized and applied for selective recognition of Hg²⁺ in aqueous/acetonitrile (1:1, v/v, pH 7) solution by employing its photophysical properties. Low toxicity and precise cell-permeability of ligand was used to probe in vitro intracellular mercury contamination using L-929 cells (mouse fibroblast cells) and BHK-21 (hamster kidney fibroblast) through confocal fluorescence microscopic experiment and bio-imaging results showed the equal applicability of ligand toward both tested cell lines. Meanwhile, it exhibited distinct Hg²⁺ induced increment in the fluorescence and absorption intensity with induction of apparent colorimetric change from colorless to reddish pink, providing naked eye mercury detection based on the metal-promoted intramolecular electronic rearrangement in probe molecule. The probe responds selectively to Hg²⁺ over various competitive cations (Sc³⁺, Yb³⁺, In³⁺, Ce³⁺, Sm³⁺, Cr³⁺, Sn²⁺, Pb²⁺, Fe²⁺, Ni²⁺, Co²⁺, Cu²⁺, Ba²⁺, Ca²⁺, Mg²⁺, Ag⁺, Cs⁺, Cu⁺, K⁺) with marked fluorogenic response and selective colorimetric changes with high sensitivity of 30 nM. We expect that the proposed method will serve as a practical tool for environmental samples analysis and biological studies.

1. Introduction

Contamination of the environment with heavy metal ions has created a pressing public health concern in living systems. Mercury is widely considered to be one of the most hazardous pollutants and highly dangerous elements due to its recognized accumulative and toxic characters in the environment and the ecosystem possesses no benign effect.¹ The widespread contamination of pollutants could jeopardize into the ecosystem, imposing a great threat to human health.² The toxicity of Hg²⁺ is related to the fact that biological ligands such as proteins, DNA, and enzymes can coordinate with mercury due to its high affinity to the thiol group in proteins.^{3,4} When Hg²⁺ is absorbed in the human body from the environment, it induces aberrations in microtubules, ion channels, mitochondria presumably and significant damage to the kidneys, heart, brain, stomach, intestines, central nervous system and endocrine systems.⁵⁻⁷ Mercury contamination occurs through a variety of natural and

anthropogenic sources including coal-fired power plants, oceanic and volcanic emissions, gold mining, combustion of waste, solid waste incineration, wood pulping, fossil fuel combustion, and chemical manufacturing.^{8,9} This metal has a relatively long atmospheric residence time because of its non-biodegradation, once mercury released into the environment, it can only be diluted or transformed, which results in long-range transport and homogenization on a hemispherical scale.¹⁰ Mercury is considered highly toxic because both elemental and ionic mercury can be converted into methyl mercury by the marine bacteria in the environment, which subsequently bio accumulates in large predatory fish, such as tuna and swordfish, consumed by humans.^{11,12} Methyl mercury is lipophilic, readily absorbed through the gastrointestinal tract, and a potent neurotoxin can cause severely deleterious health effects for human beings and has been implicated as a cause of prenatal brain damage, various cognitive and motion disorders, and Minamata disease;¹³ when ingested by a pregnant woman, methyl mercury readily crosses the placenta and targets the developing fetal brain and central nervous system, which can cause developmental delays in children.¹⁴

^a Department of Chemistry, Kongju National University, Gongju, Chungnam 314-701, Republic of Korea

^b Department of Plasma Bioscience and display, Kwangwoon University, 20 Kwangwoon-gil, Nowon-gu, Seoul 139-701, Republic of Korea

Given these environmental and toxicological concerns, much effort has been devoted to develop new mercury detection strategies for use in aqueous solution and in biological samples.¹⁵ Although traditional analytical techniques including atomic absorption spectroscopy, atomic fluorescence spectrometry,¹⁶ dispersive liquid–liquid microextraction,¹⁷ inductively coupled plasma atomic emission spectrometry, electrochemical sensing, and the use of piezoelectric quartz crystals make it possible to detect low limits.^{18,19} However, these methods require expensive equipment and involve time-consuming and laborious procedures that can be carried out only by trained professionals. Alternatively, applying fluorescent sensors to detect heavy metal ions are favored over other common analytical methods due to their favorable features of operational simplicity, cost-effectiveness, high sensitivity and selectivity, quick response, and high temporal resolution.²⁰ Therefore, fluorogenic chemosensors are excellent candidates to probe mercury in the environmental and physiological samples.^{21,22} A number of fluorescent molecular probes based on the coordination of heteroatom-based ligands to Hg²⁺ have been reported in recent years, enabling easy detection of mercury ions.^{23–27}

Recently, rhodamine derivatives have received increasing attention in the design of chemosensors for metal ions.^{28–30} However; more improvements for these rhodamine-based sensors are still in demand to be compatible with biological and environmental applications. The major drawbacks that limit the practical use of a sensor are low water solubility, low fluorescence quantum yield in aqueous media, difficult surface conjugation chemistry and cross sensitivities toward other metal cations. Therefore, it still remains a great challenge and ever-growing demand to develop some simple, rapid responsive, sensitive and specific Hg²⁺ detection assays, suitable for quick determination in drinking water, food resources and mercury accumulation in living cells with less toxicity for practical use.^{31–34}

In this regard, ligand that can provide optical feedback on binding to the Hg²⁺ in aqueous or mixed aqueous environments in the form of visually detectable change in color and fluorescence are expected to find applications both as colorimetric staining agents for easy and facile detection; and as fluorescent imaging reagents for the biological cells that are affected with Hg²⁺ adsorption.^{35,36} Moreover, the fluorescence imaging technique can map the distribution of guest species within living cells. Since, rhodamine-based chemosensors have been widely used for detecting intracellular analytes.^{37–41} In the present study, we have explored the applicability of our design ligand for in vitro monitoring of mercury ions in aqueous solution as well as in living cells using L-929 cells (mouse fibroblast cells) and BHK-21 (hamster kidney fibroblast) under confocal fluorescence microscopy. The results showed good compatibility of synthesized ligand toward Hg²⁺ detection in aqueous solution and living cells with nano molar concentration level which suggest the utility of ligand as the fluorogenic signal reporting platform for Hg²⁺. The findings suggest that this method will serve as the foundation of practical chemosensor for rapidly determining Hg²⁺ contamination in intracellular and aqueous system owing satisfactory aqueous/acetonitrile solubility, low toxicity, convenient synthetic procedure, high sensing specificity for Hg²⁺ over other competing cations at ambient temperature under neutral pH condition.

2. Experimental

2.1. Substrate and reagents

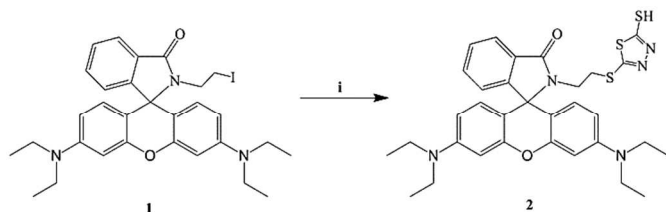
Rhodamine B, 1,3,4-thiadiazole-2,5-dithiol, K₂CO₃, POCl₃, were purchased from Aldrich. Triethyl amine, ethanol, methanol, 1,2-dichloroethane, acetonitrile, acetone, water, dimethyl sulfoxide, hexane and ethyl acetate (Samchun chemicals, Korea), and Sc(OTf)₃, YbCl₃·6H₂O, InCl₃, CeCl₃, SmCl₃·6H₂O, CrCl₃·6H₂O, SnCl₂, PbCl₂, FeCl₂·nH₂O, NiCl₂·6H₂O, CoCl₂·6H₂O, CuCl₂·2H₂O, BaCl₂·2H₂O, CaCl₂·2H₂O, CsCl, CuCl, KCl (Aldrich and Alfa Aesar) were used during experiment. The major chemicals utilized for biological studies includes MEM (minimum essential media, Wel Gene, Korea), FBS (fetal bovine serum, Bio west U.S.A), Tripsin (Thermo scientific, South Loga, Utah), PBS (Wel Gene, Korea) and MTT [3-(4,5-dimethylthiazol-2-yl)-2,5-diphenyltetrazoliumbromide, Sigma Aldrich, U.S.A].

2.2. Instrumentations

The reaction progress was monitored by thin layer chromatographic (TLC) analysis, and the R_f values were determined by employing pre-coated silica gel aluminum plates, Kieselgel 60 F254 from Merck (Germany), using *n*-hexane : ethyl acetate, 1:1 as an eluent. TLC was visualized under a UV lamp (VL-4. LC, France). The FT-IR spectra were recorded in KBr pellets on a SHIMADZU FTIR-8400S spectrometer (Kyoto, Japan). Proton and carbon nuclear magnetic resonance (¹H NMR & ¹³C NMR) spectra were recorded on a Bruker Avance 500 MHz spectrometer with TMS as an internal standard. The chemical shifts are reported as δ values (ppm) downfield from the internal tetramethylsilane of the indicated organic solution. Peak multiplicities are expressed as follows: s, singlet, bs, broad signal, t, triplet, q, quartet and m, multiplet. The coupling constants (*J* values) are given in hertz (Hz). Mass spectra were recorded on the AB SCIEX Co. 4000 QTRAP LC/MS/MS System. Abbreviations are used as follows: DMSO-*d*₆, Dimethyl sulfoxide-*d*₆; FT-IR spectroscopy, Fourier transform infrared spectroscopy.

2.3. Chemistry

Formation of the ligand **2** was indicated by FT-IR spectrum due to appearance of broad signal at 2370 cm⁻¹ characteristic for terminal –SH stretching vibration of 2,5-dimercapto thiadiazole; while absorption band for the C=N stretching vibration at 1585 cm⁻¹ and C–S stretching vibration at 1230 cm⁻¹ indicate the attachment of mercapto thiadiazole ring to the rhodamine B derivative **1** (Supporting information, Fig. S5). Further confirmation was carried out through ¹H NMR and ¹³C NMR spectra by the appearance of broad signal at 14.48 ppm due to terminal –SH group and additional signals in the aromatic as well as aliphatic region of both ¹³C NMR and ¹H NMR spectra (Supporting information, Fig. S1.2). In the mass spectral data, molecular ion peak [M+H]⁺ at *m/z* = 618 indicates the correct mass of **2** (Supporting information, Fig. S7). The reaction pathway adopted for the synthesis of **2** was outlined in Scheme 1.



Scheme 1: Synthesis of ligand **2**: Reagents and conditions. (i) 1,3,4-Thiadiazole-2,5-dithiol, K_2CO_3 , ethanol, reflux 10 h.

2.4. General procedure for the synthesis of ligand **2**

3',6'-Bis(diethylamino)-2-(2-iodoethyl)spiro[isoin-doline-1,9'-xanthen]-3-one (**1**) was prepared by reported procedure.⁴² Then compound **1** (1.4 g, 2.35 mmol) and 1,3,4-thiadiazole-2,5-dithiol (0.35 g, 2.35 mmol) was stirred in ethanol (60 mL). After addition of K_2CO_3 (0.97 g, 7.05 mmol) the reaction mixture was heated under reflux for 10 h, monitored by TLC. After consumption of starting material, the reaction mixture was cooled to room temperature and filtered. Filtrate after evaporation under reduced pressure left crude **2** as white solid on cooling, which was purified by column chromatography and crystallized on methanol.

2.5. 3',6'-Bis(diethylamino)-2-[2-[(5-mercapto-1,3,4-thiadiazol-2-yl)thio]ethyl]spiro(isoin-doline-1,9'-xanthen)-3-one (**2**)

White solid; yield: 64 %; R_f : 0.81 (*n*-hexane : ethyl acetate, 1:1); 1H NMR (500 M Hz, $DMSO-d_6$) δ 14.48 (bs, 1H, SH), 7.83–7.80 (aromatic, 1H, m), 7.58–7.51 (aromatic, 2H, m), 7.10–7.06 (aromatic, 1H, m), 6.40–6.34 (xanthen, 6H, m), 3.36–3.18 (aliphatic, 8H, q, $J = 8$ Hz), 2.80–2.76 (aliphatic, 2H, t, $J = 10$ Hz), 2.52–2.50 (aliphatic, 2H, t, $J = 7.5$ Hz), 1.11–1.07 (aliphatic, 12H, t, $J = 10$ Hz); ^{13}C NMR (125 MHz, $DMSO-d_6$) δ 188.3, 167.4, 157.7, 153.4, 153.1, 133.4, 130.7, 128.9, 128.8, 124.2, 122.9, 108.7, 97.6, 64.4, 44.2, 38.7, 32.2, 12.8; MS for $C_{32}H_{35}N_5O_2S_3$ (ESI, *m/z*), 618 $[M+H]^+$.

2.6. Ligand-metal chelation

Recently, considerable efforts have been made to propose the metal induced ring opening mechanism of rhodamine derivatives.^{16, 43-47} To understand the chelation mechanism of ours synthesized ligand **2** with mercury ion, 1H NMR titration and FT-IR spectral analysis before and after metal complexation with the ligand was performed to get insight into the ligation mode of **2** to Hg^{2+} , which verify the involvement of mercapto thiadiazole to the complex formation reaction. There was a broad signal at 2370 cm^{-1} due to terminal -SH stretching vibration in the ligand before reaction with the mercury ion, while this signal suppressed after ligand-mercury chelation, give indication about terminal -SH involvement in the mercury ligation as sulfur exhibited strong affinity toward mercury.^{15,48} Furthermore, there was a slight shift in the spiro-lactam carbonyl stretching vibration from 1743 cm^{-1} to 1686 cm^{-1} give indication of carbonyl oxygen involvement in the ligand-mercury complexation reaction (Supporting information, Fig. S5,S6). While in case of 1H NMR spectra, there was a significant change in the ethylene proton signal at 3.33–3.18 ppm before and after mercury chelation considered due to transformation of neighbouring tertiary

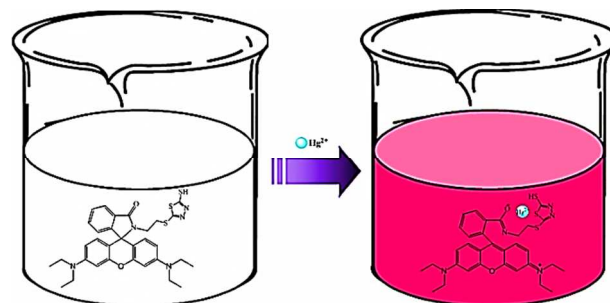


Fig. 1 Proposed spiro-lactam ring opening mechanism of ligand **2** upon mercury chelation in acetonitrile/water (1:1, v/v) at pH 7.0.

amine to ammonium ion through electronic delocalization; meanwhile, significant signal variation in xanthen proton of rhodamine B backbone at 6.40–6.34 ppm attributed to the delocalization of electronic cloud after mercury induced spiro-lactam ring opening of the ligand, and disappearance of -SH signal at 14.48 ppm confirm the involvement of terminal -SH in the ligand-mercury complexation reaction (Supporting information, Fig. S1–4). In the mass spectrum, a characteristic signal at *m/z* 618 corresponding to $[M+H]^+$ was clearly observed give correct mass of ligand **2** (Supporting information, Fig. S7). Furthermore, there was a considerable mass increment from *m/z* 618 to *m/z* 818 after mercury chelation with ligand give correct mass of ligand-mercury complex (Supporting information, Fig. S8). On the basis of these observations, the proposed ligand-mercury chelation mechanism is shown in Fig. 1.

3. Results and discussions

3.1. Spectroscopic properties

It is well known that sulfur and nitrogen can act as soft binding sites for metal cations.³ Mercury ions have a strong ability to bind with sulfur atoms.^{45,49-50} Initially, based on these binding abilities of Hg^{2+} , we tried to synthesize a mercapto thiadiazole substituted rhodamine B derivative **2** and explored its potential for selective signaling of Hg^{2+} in aqueous solution and living cells which was found to bind strongly and selectively with Hg^{2+} . Fluorescence and UV-visible spectral response of ligand were monitored upon adding Hg^{2+} to determine the cations binding ability of ligand. Ligand alone does not exhibit any fluorescence or UV-visible response in the range of 550–600 nm in the absence of metal ions. A high intensity fluorescence emission band at 587 nm and UV-visible absorption band at 554 nm were observed upon addition of Hg^{2+} into the aqueous/acetonitrile (1:1, v/v, pH 7.0) solution of ligand **2** with significant color change from colorless to reddish pink, suggesting the conversion of ligand into spiro-lactam ring opened xanthen conformation triggered by activation of spiro-lactam carbonyl group with mercury ion. The newly generated delocalized xanthen conformation of the ligand has extended conjugation that overall decrease the energy gap between HOMO to LUMO, and, thus causing rapid electronic transition at low energy exhibiting emission and absorption in the visible range (Fig. 2). Consequently, coordination reaction was monitored by using different mercury salts in order to assess the effect of counter ion on the fluorescence and

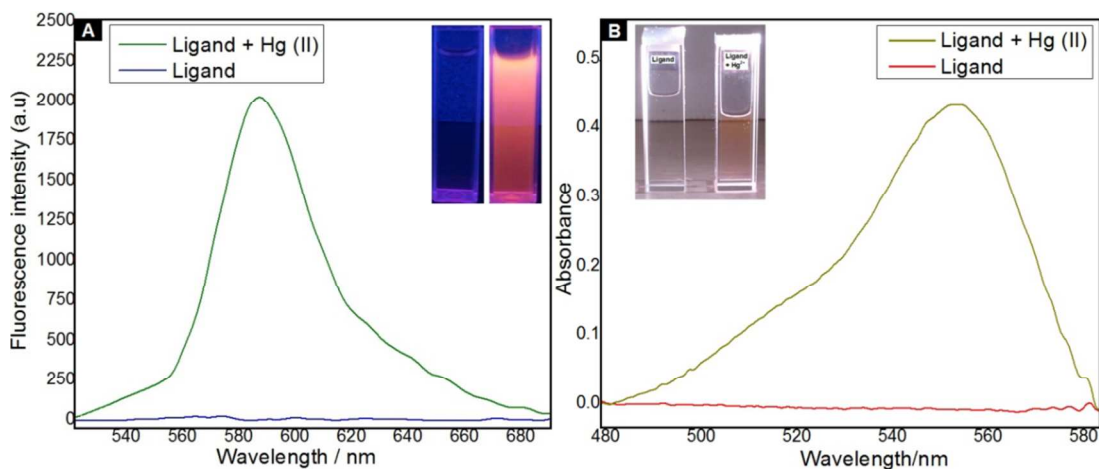


Fig. 2 (A) Fluorescence emission spectrum of ligand **2** (0.03 μM) in the presence and absence of Hg^{2+} (0.06 μM) in acetonitrile/water (1:1, v/v) at pH 7.0; Inset photograph described the colorimetric change (under UV light, 365 nm) before and after $\text{Hg}(\text{ClO}_4)_2$ addition into ligand solution; (B) UV-visible absorption spectrum of ligand **2** (0.06 μM) in the presence and absence of Hg^{2+} (0.12 μM) in acetonitrile/water (1:1, v/v) at pH = 7.0. Inset photograph described the colorimetric change (under ambient light)

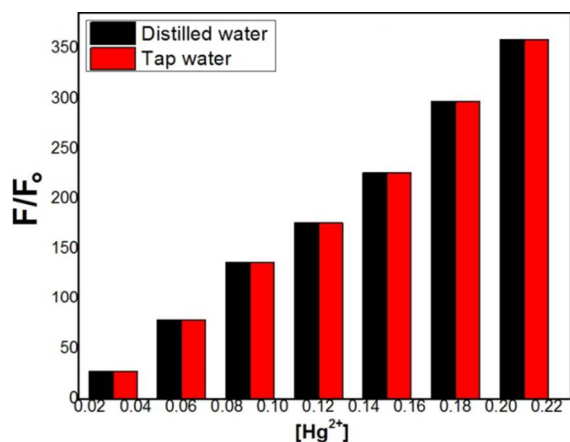


Fig. 3 Fluorescence emission spectral enhancement of ligand **2** (0.03 μM) in the presence of Hg^{2+} (0.03–0.21 μM , 1–7 equivalents) in acetonitrile/water (1:1, v/v) at pH 7.0; black bars represent the fluorescence response of ligand solution prepared in distilled water and red bars represent the fluorescence intensity variation of ligand solution prepared in tap water.

UV-visible absorption spectra. Similar results were obtained when different mercury salts, such as HgCl_2 and $\text{Hg}(\text{ClO}_4)_2$, were employed, therefore, it appears that counter ions have no effect on chemosensor electronic spectra before and after $\text{Hg}(\text{ClO}_4)_2$ addition into ligand solution.

A colorimetric sensor is especially promising because the color change can be easily observed by naked eye, thus less work and no costly equipments are required. Therefore, the colorimetric behavior of ligand was also investigated under the same conditions using distilled water as well as tap water for practical use. The selectivity of this system as a visual colorimetric sensor for Hg^{2+} over other metal ions is evident as only Hg^{2+} shows a significant color change, whereas all other metal ions remain colorless without any perceptible change (Supporting information, Fig. S9), while the same fluorescence enhancement was observed for the test solution prepared in distilled and tap water (Fig. 3).

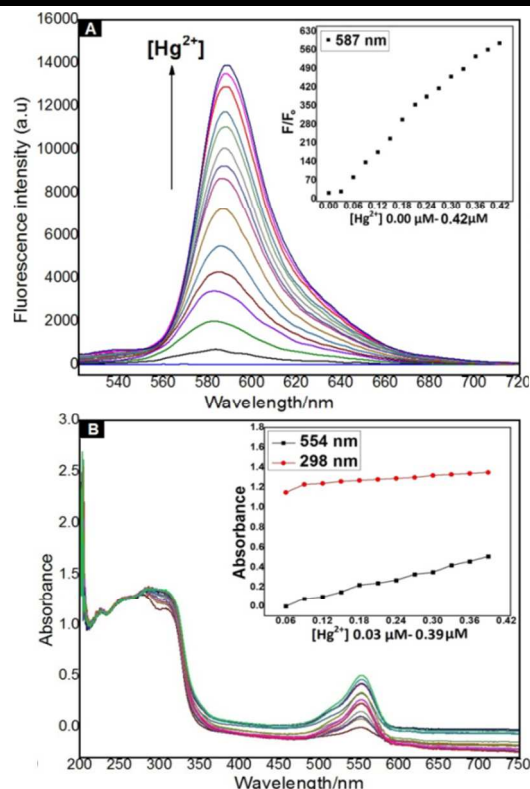


Fig. 4 (A) The fluorescence titration of ligand **2** (0.03 μM) at emission maxima of 587 nm as a function of mercury concentration (0–0.42 μM , 0–14 equivalent), the inset described the fluorescence enhancement at emission maxima of 587 nm; F/F_0 is determined as a ratio between the maximum fluorescence intensity (F , after Hg^{2+} addition) and minimum fluorescence intensity (F_0 , free ligand solution in absence of Hg^{2+}); (B) Absorption spectrum of ligand **2** (0.06 μM) with increasing concentration of mercury ion ranging from 0.06–0.42 μM (1–7 equivalent), in methanol/water (1:1, v/v) at pH 7. The inset shows titration curve by absorbance at 554 nm while there was a slight variation at 298 nm.

3.1.1. Fluorescence and UV-visible titration

To gain more insight into the behavior of **2** towards Hg^{2+} , the fluorescence and UV-visible titration experiment was conducted

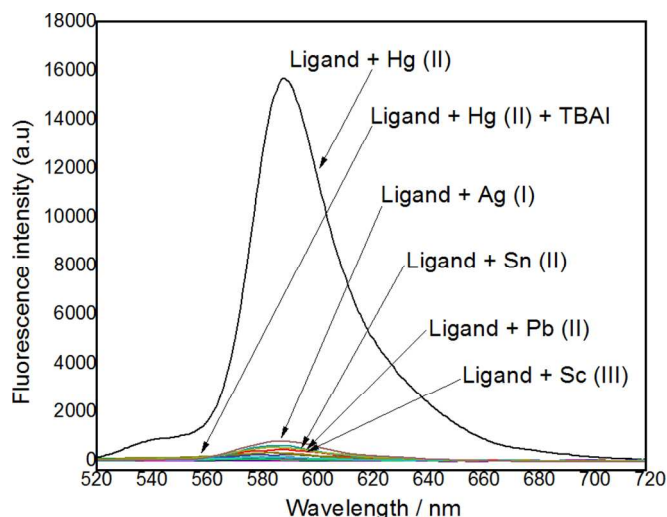


Fig. 5 Fluorescence emission spectrum of ligand (0.03 μM) in the presence of Hg^{2+} (0.5 μM) and competing ions (Sc^{3+} , Yb^{3+} , In^{3+} , Ce^{3+} , Sm^{3+} , Cr^{3+} , Sn^{2+} , Pb^{2+} , Fe^{2+} , Ni^{2+} , Co^{2+} , Cu^{2+} , Ba^{2+} , Ca^{2+} , Mg^{2+} , Ag^{+} , Cs^{+} , Cu^{+} , K^{+}) (0.5 μM) in aqueous/acetonitrile (1:1, v/v) at pH 7.0, while mercury ligation become reversible in excess addition of TBAI into ligand- Hg^{2+} solution.

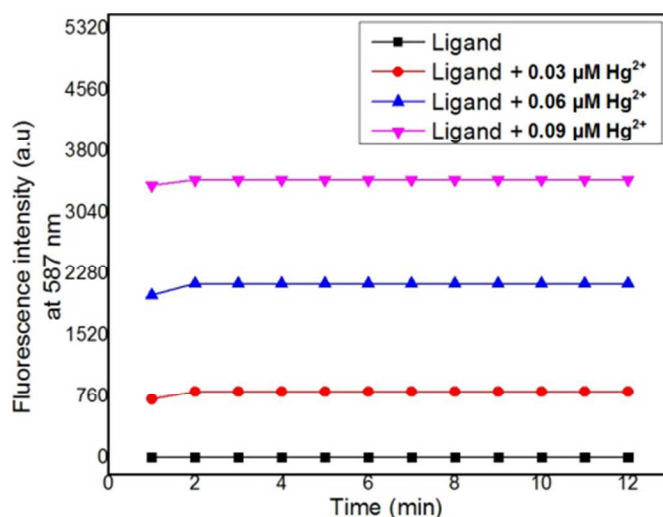


Fig. 6 Effects of reaction times on the fluorescent intensity of ligand (0.03 μM) at maximum emission of 587 nm in the presence of Hg^{2+} (0.03–0.09 μM) in aqueous/acetonitrile, (1:1, v/v) at neutral pH condition.

which revealed that the fluorescence intensity of ligand solution gradually increased with increasing concentration of mercury ions in aqueous/acetonitrile (1:1, v/v) at neutral pH condition. A linear relationship was obtained between the fluorescence intensity at 587 nm upon increasing concentration of mercury ions ranging from 0.03 μM –0.42 μM (Fig. 4A) and the value of linearly dependent co-efficient (R^2) was found to be 0.99347 (inset of Fig. 4A). From this titration experiment, the detection limit of chemosensor was estimated to be about 30 nM. The same results was obtained by the electronic spectra obtained from UV–visible titration experiment of ligand as a function of Hg^{2+} concentration as shown in Fig. 4B. There was a continuous increment in absorption intensity with maximum absorption at 554 nm by increasing Hg^{2+} concentration.

3.1.2. Selectivity of ligand toward Hg^{2+} over competing ions

To assess the specificity of synthesized chemosensor, various ions including heavy metal ions, were examined in parallel under the same condition. As depicted from Fig. 5, the reaction of ligand with Hg^{2+} produces strong fluorescence response; whereas miscellaneous competitive metal ions do not show this behavior. However, there was a negligible response toward other less thiophilic cations, for example, Ag^{+} , Sn^{2+} , Pb^{2+} and Sc^{3+} , although not so sensitive but there was slight signal appearance with no colorimetric change. However, huge difference between intensity of ligand chelation with Hg^{2+} and competing ions is considerably enough to detect the relevant concentration of Hg^{2+} in aqueous/acetonitrile (1:1, v/v, pH 7) sample. Furthermore, reversibility of chemosensor **2** was verified by the immediate disappearance of solution color and fluorescence quenching upon excess addition of tetrabutylammonium iodide (TBAI) into the mixture of **2** and Hg^{2+} (Fig. 5).

3.1.3. Effect of time on ligand- Hg^{2+} chelation

To understand the response rate of fluorescent signal and ligand- Hg^{2+} reaction time upon addition of Hg^{2+} , the fluorescent intensity of ligand was measured at different time intervals. The time dependent response of ligand toward Hg^{2+} revealed that the reaction of ligand **2**

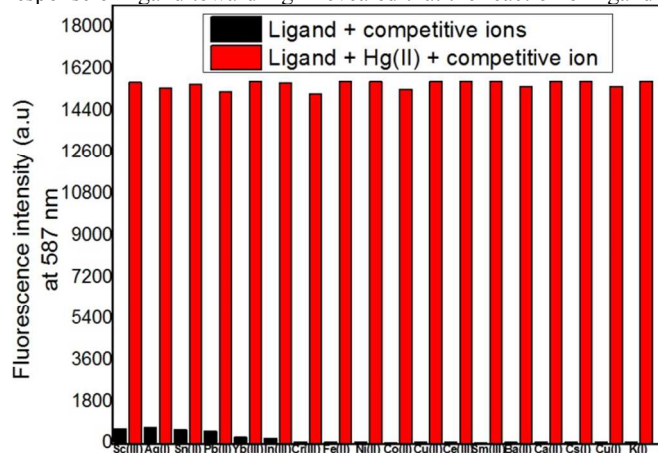


Fig. 7 The fluorescence intensity contrast bars in order to investigate the interference effect of other metal ions (Sc^{3+} , Yb^{3+} , In^{3+} , Ce^{3+} , Sm^{3+} , Cr^{3+} , Sn^{2+} , Pb^{2+} , Fe^{2+} , Ni^{2+} , Co^{2+} , Cu^{2+} , Ba^{2+} , Ca^{2+} , Mg^{2+} , Ag^{+} , Cs^{+} , Cu^{+} , K^{+}) on the detection ability of ligand for Hg^{2+} , red bars represent the fluorescence response of ligand (0.03 μM) to Hg^{2+} (0.5 μM) in the presence of interfering metal ions (0.5 μM) and black bars represent the fluorescence intensity of ligand (0.03 μM) with competing ions (0.5 μM) in the absence of Hg^{2+} .

with Hg^{2+} started immediately, as there was a sudden change in fluorescence intensity, and completed within few second. The fluorescence intensity becomes constant within 2 minutes (Fig. 6).

3.1.4. Fluorescence response of ligand- Hg^{2+} solution upon addition of competing cations

To assess the possible interference by other metal ions on the fluorescence intensity of ligand- Hg^{2+} solution, the fluorescence changes of ligand (0.03 μM) with Hg^{2+} (0.5 μM) and miscellaneous cations (0.5 μM) including Sc^{3+} , Yb^{3+} , In^{3+} , Ce^{3+} , Sm^{3+} , Cr^{3+} , Sn^{2+} ,

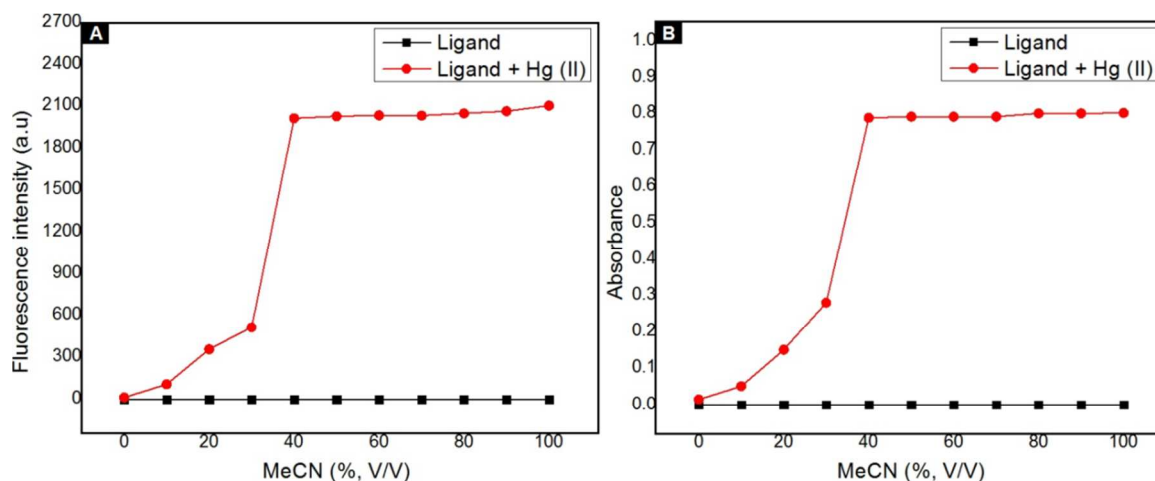


Fig. 8 (A) Variation of fluorescence intensity of ligand **2** ($0.03 \mu\text{M}$) with and without mercury ion ($0.06 \mu\text{M}$) at 587 nm upon different water : acetonitrile, ratio; while base line signal are due to only ligand without metal addition in aqueous/acetonitrile solvent system; (B) Variation of absorption intensity of ligand **2** ($0.06 \mu\text{M}$) with and without mercury ion ($0.5 \mu\text{M}$) at 587 nm upon different water : acetonitrile, ratio at ambient temperature under neutral pH condition and base line signal are due to only ligand without metal addition in aqueous/acetonitrile solvent system.

Table 1: Solvent effect on the mercury–ligand chelation

S. No.	Solvent	$^aF/F_0$	Emission maxima (nm)	bA	Absorption maxima (nm)	Stokes shift (cm^{-1})
1	Water	08	587	0.020	554	1014
2	MeCN : H_2O (1:1, v/v)	176	587	0.420	554	1014
3	MeOH : H_2O (1:1, v/v)	156	587	0.401	554	1014
4	EtOH : H_2O (1:1, v/v)	148	587	0.401	554	1014
5	DMSO : H_2O (1:1, v/v)	122	587	0.302	554	1014

$^aF/F_0$ = Fluorescence intensity of $0.03 \mu\text{M}$ ligand at emission maxima 587 nm , in the presence and absence of $0.12 \mu\text{M}$ Hg^{2+} .

bA = Absorption signal intensity of $0.06 \mu\text{M}$ ligand at absorption maxima 554 nm , in the presence of $0.12 \mu\text{M}$ Hg^{2+} .

Pb^{2+} , Fe^{2+} , Ni^{2+} , Co^{2+} , Cu^{2+} , Ba^{2+} , Ca^{2+} , Mg^{2+} , Ag^+ , Cs^+ , Cu^+ and K^+ in acetonitrile/water (1:1, v/v, pH 7) were measured. The tested background metal ions showed small or no interference with the detection of Hg^{2+} (Fig. 7). Moreover, the miscellaneous competitive cations did not lead to any significant fluorescence changes. These facts suggested that ligand could recognize Hg^{2+} with high selectivity against other metal ions under physiological conditions and excess of competing cations did not obviously influence the detection of Hg^{2+} in aqueous/acetonitrile, 1:1, solution.

3.1.5. Solvent effect on ligand–mercury response mechanism

The effect of water contents on the fluorescence and UV–visible spectral measurement of ligand with Hg^{2+} were investigated, as shown in Fig. 8. The cation sensing ability of the sensor varies with the volume ratio of water. It can be observed that the sensor **2** exhibited sensitive response to Hg^{2+} in aqueous/acetonitrile, (1:1, v/v) solvent system, the fluorescence emission and absorption signal intensity gradually increased and reached to maximum value at approximately, 40 % aqueous/acetonitrile solvent system while further increase in acetonitrile content bring slight change in signal intensity at 587 nm in case of fluorescence and at 554 nm in UV–visible absorption measurement, and become stable above 50 % aqueous acetonitrile solution. Inspiring from these results, 50 % aqueous/acetonitrile media was selected for the fluorescence excitation, emission and UV–visible spectral recording; while ligand

alone showed no emission and absorption signal at 587 nm and 554 nm , respectively, with the used solvent system at neutral pH condition.

The coordination reaction was greatly dependent on the nature of solvent; organic solvent exert significant effect on the absorption and emission intensity, maximum absorption response was observed in

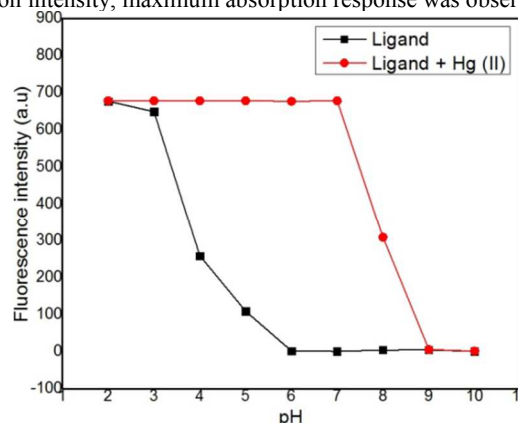


Fig. 9 Fluorescence intensity variation at maximum emission of 587 nm , with alteration of pH from 2 to 10 in buffer solution.

mixed acetonitrile water (1:1, v/v) solution. The effect of different aqueous organic solvent on the emission and absorption intensity upon chelation of mercury ion with ligand is tabulated in Table 1.

3.1.6. pH effect on ligand–mercury chelation

For practical applicability, the proper pH condition of synthesized chemosensor was evaluated by recording the fluorescence spectra in buffer with pH range of 2 to 10 as shown in Fig. 9. The ring opening of free rhodamine B derivative **2** took place spontaneously under acidic conditions (pH <5) because of the strong protonation of spirolactam carbonyl by acid while rhodamine B derivative **2** (ligand) spirolactam ring remain stable at neutral pH and did not show any fluorescence and absorption signal under neutral pH condition due to existence of ligand in spirolactam conformation with localized electronic cloud. When the pH of solution was over 5, no acid induced ring opening of **2** was observed. However, in the presence of Hg²⁺, there was an obvious fluorescence off–on change between pH 5 and 8 which was attributed to the opening of the spirolactam ring of ligand triggered by mercury chelation. However, around pH 7, the F/F₀ value reached maximum, indicating that **2** possessed the highest sensing ability in a physiological environment, which was more fruitful for cell imaging study that required nearly neutral pH condition. These results indicate that the optimal pH span for ligand sensation is 5.0–8.0. This property of ligand **2** suggests that no buffer solutions are required for the detection of Hg²⁺, which is convenient for practical application to probe mercury in drinking water and biological fluid under neutral pH.

3.1.7. Stokes shift

The difference between positions of band maxima of excitation and emission spectra of the same electronic transition is called Stokes shift. The ligand **2** after mercury chelation exhibited significant Stokes shift of 1014 cm⁻¹ for easy separation of excitation and emission signal, (Fig. 10) calculated by the equation 1,⁵¹ in aqueous/acetonitrile (1:1, v/v, pH 7) solution. The larger Stokes shift and longer wavelength chromophore considered to be more compatible for sensing and intracellular cell imaging.⁵²⁻⁵⁵

$$(\nu_A - \nu_F) = \left(\frac{1}{\lambda_A} - \frac{1}{\lambda_F} \right) \times 10^7 \dots\dots\dots (1)$$

Where ν_A and ν_F are the absorption and fluorescence frequencies, λ_A and λ_F are the absorption maxima and fluorescence emission maxima, respectively.

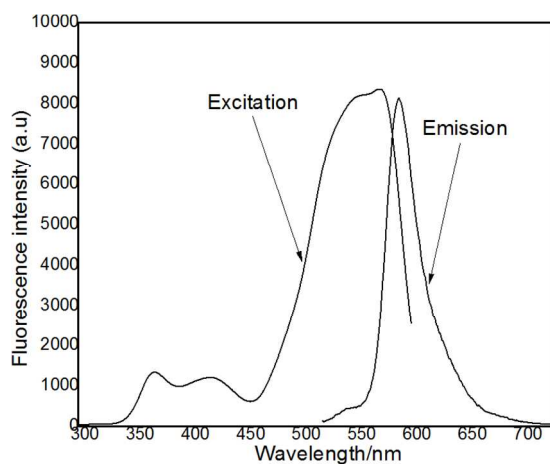


Fig. 10 Fluorescence excitation and emission spectrum of **2** in the presence of Hg²⁺ in aqueous/acetonitrile (1:1, v/v) at pH 7.0

3.1.8. Fluorescence quantum yield determination

Fluorescence quantum yield of ligand-Hg²⁺ complex solution was calculated to be $\Phi_{FL} = 0.54$ (relative to the standard rhodamine B in acetonitrile, $\Phi_{std} = 0.59$),⁵⁶ using equation 2.⁵⁷

$$\Phi_{unk} = \Phi_{std} (I_{unk}/A_{unk})(A_{std}/I_{std})(\eta_{unk}/\eta_{std})^2 \dots\dots\dots (2)$$

Where Φ_{unk} is the fluorescence quantum yield of the sample, Φ_{std} is the quantum yield of the standard, I_{unk} and I_{std} are the integrated fluorescence intensities of the sample and the standard, respectively, A_{unk} and A_{std} are the absorbance's of sample and the standard at the absorption wavelength, respectively, η_{unk} and η_{std} are the refractive indices of corresponding solutions.

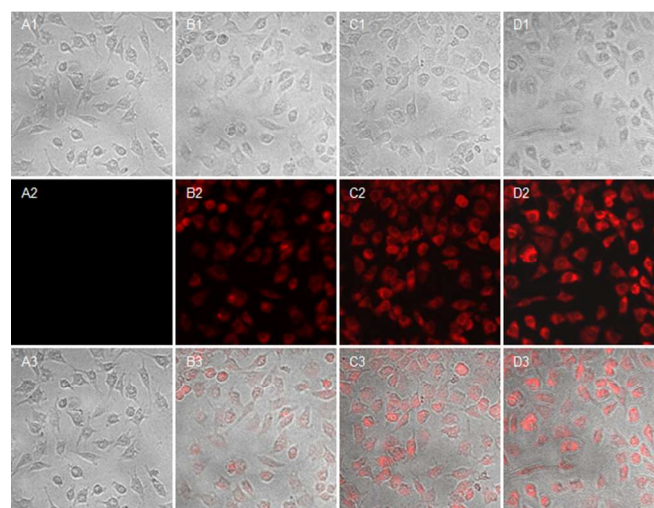


Fig. 11 Confocal fluorescence microscopic images for L-929 cells; (A1-A3) L-929 cells incubated with probe (1.5 μM); (B1-B3) L-929 cells incubated with probe (1.5 μM) in the presence of (1.25 μM) mercuric ion; (C1-C3) L-929 cells incubated with probe (1.5 μM) in the presence of (2.5 μM) mercuric ion; (D1-D3) L-929 cells incubated with probe (1.5 μM) in the presence of (5 μM) mercuric ion. A1-D1: Bright field images; A2-D2: fluorescence images; A3-D3: merged images.

3.2. Bioimaging applications of ligand **2** in L-929 and BHK-21 cell lines

3.2.1. Bio-imaging applications of ligand **2** in L-929 cells (mouse fibroblast cells)

To investigate the capability of the ligand **2** to track the change in Hg²⁺ level within biological samples, the fluorescence imaging experiments were performed following the reported procedure⁵⁸ with some modifications. Briefly, L-929 cells (mouse fibroblast cells) and BHK-21 (hamster kidney fibroblast) were incubated with ligand **2** (1.5 μM) in complete MEM (minimum essential media) for 4 hours at 30 °C, then very fragile fluorescence was observed in both cell

ARTICLE

lines. After washing with PBS twice, the samples were treated with Hg^{2+} in different concentrations ranging from 1.5-5 μM for more than 30 min at 37 $^{\circ}\text{C}$, which displayed distinct intracellular fluorescence depending on the Hg^{2+} concentrations. The results of bioimaging experiments against L-929 are shown in Fig. 11.

3.2.2. Bioimaging applications of ligand 2 in BHK-21 (hamster kidney fibroblast)

As the major accumulation of mercury inside the human body takes place in the kidney as compared to other body organs such as liver and brain, furthermore, the renal toxicity caused by mercury is widely documented in literature.⁵⁹⁻⁶⁴ Meanwhile, thiol-dependent nuclear factor KB (NF-KB) controls the apoptotic stimulus and promotes cell survival. Mercuric ions are well known thiol-binding agent which impairs the NF-KB function in kidney epithelial cells leading to the cell death.⁶⁵ These finding inspired us to further investigate the bioimaging studies utilizing BHK-21 (hamster kidney fibroblast). However, ligand 2 was successfully applied for the fluorescent imaging of Hg^{2+} inside hamster kidney fibroblast cells (Fig. 12). From this experiment, we concluded that the synthesized ligand 2 can be used to probe mercury in multiple cell lines with promising fluorescence response.

3.3. Cytotoxicity evaluation

Moreover, to assess the toxicity level, MTT assay was performed after 4, and 24 hours of ligand 2 treatment. BHK-21 cells showed little toxic effect at 4 hours while L-929 cells exhibited no toxicity as shown in Fig. 13A and B, respectively.

4. Conclusion

In summary, we have devised an efficient ratiometric fluorescent probe 2 for mercury sensation based on the metal-promoted spirolactam ring opening of synthesized ligand, exhibiting potent binding affinity for mercury ion showing strong absorption band at 554 nm and fluorescence emission at 587 nm with distinct color change of solution for naked eye detection, while common metal ions (Sc^{3+} , Yb^{3+} , In^{3+} , Ce^{3+} , Sm^{3+} , Cr^{3+} , Sn^{2+} , Pb^{2+} , Fe^{2+} , Ni^{2+} , Co^{2+} , Cu^{2+} , Ba^{2+} , Ca^{2+} , Mg^{2+} , Ag^{+} , Cs^{+} , Cu^{+} , K^{+}) do not interfere the detection of mercury with ligand reflecting the stronger competition binding ability of mercury toward the ligand investigated in aqueous/acetonitrile (1:1, v/v) at pH 7.0. Furthermore, quick response toward mercury chelation with promising selectivity, high detection sensitivity, less toxicity, satisfactory solubility in mixed solvent, switchable photophysical properties and easy preparative protocol of proposed sensing system make it a reliable platform for nano molar mercury detection in aqueous solution and living cells. The bio-imaging results showed the equal applicability of ligand for L-929 cells (mouse fibroblast cells) and BHK-21 (hamster kidney fibroblast) with precise cell permeability and low toxicity against the tested cell lines.

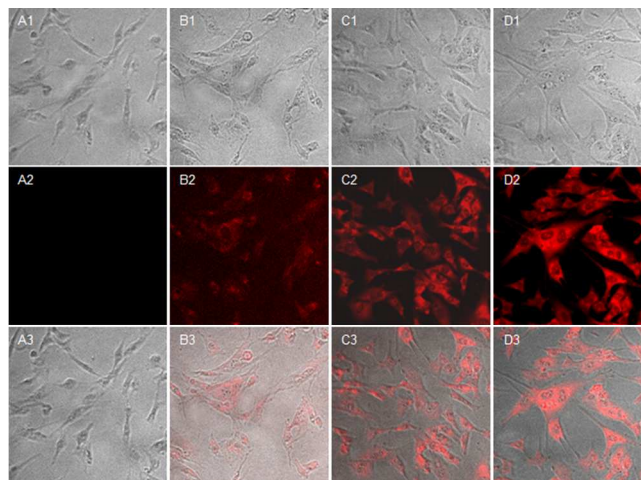


Fig. 12 Confocal fluorescence microscopic images for BHK-21 cells; (A1-A3) BHK-21 cells incubated with probe (1.5 μM); (B1-B3) BHK-21 cells incubated with probe (1.5 μM) in the presence of (1.25 μM) mercuric ion; (C1-C3) BHK-21 cells incubated with probe (1.5 μM) in the presence of (2.5 μM) mercuric ion; (D1-D3) BHK-21 cells incubated with probe (1.5 μM) in the presence of (5 μM) mercuric ion. A1-D1: Bright field images; A2-D2: fluorescence images; A3-D3: merged images.

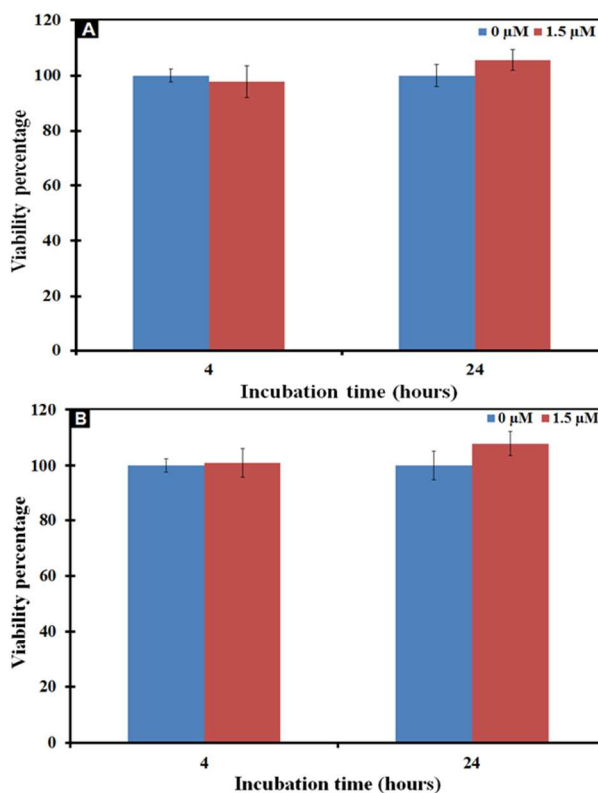


Fig. 13 Cell viability of (A) BHK-21 and (B) L-929 cells cultured in complete media with ligand 2 (1.5 μM) while the control cells were cultured in the medium without ligand.

Acknowledgements

This research was supported by the Basic Science Research Program through the National Research Foundation of Korea (NRF) funded by the Ministry of Education, Science and Technology (No. 2011-0015056) and the National Research Foundation of

1 Korea(NRF) grant funded by the Korea government(MSIP) (NRF-
2 2010-0027963).

References

1. L. Chen, L. Yang, H. Li, Y. Gao, D. Deng, Y. Wu, L. Ma, *J. Inorg. Chem.*, 2011, **50**, 10028–10032.
2. M. Santra, B. Roy, K. H. Ahn, *Org. Lett.*, 2011, **13**, 3422–3425.
3. V. Tharmaraj, K. Pitchumani, *Anal. Chim. Acta.*, 2012, **751**, 171–175.
4. A. K. Atta, S. B. Kim, J. S. Heo, D. G. Cho, *Org. Lett.*, 2013, **15**, 1072–1075.
5. Z. Zhang, X. Guo, X. Qian, Z. Lu, F. Liu, *Kidney Int.*, 2004, **66**, 2279–2282.
6. J. Huang, X. Ma, B. Liu, L. Cai, Q. Li, Y. Zhang, K. Jiang, S. Yin, *J. Lumin.*, 2013, **141**, 130–136.
7. M. Wang, X. An, J. Gao, *J. Lumin.*, 2013, **144**, 91–97.
8. E. M. Nolan, S. J. Lippard, *J. Am. Chem. Soc.*, 2003, **125**, 14270–14271.
9. E. M. Nolan, S. J. Lippard, *Chem. Rev.*, 2008, **108**, 3443–3480.
10. H. Tan, Y. Zhang, Y. Chen, *Sens. Actuators, B*, 2011, **156**, 120–125.
11. E. M. Nolan, S. J. Lippard, *J. Mater. Chem.*, 2005, **15**, 2778–2783.
12. G. Aragay, J. Pons, A. Merkoci, *Chem. Rev.*, 2011, **111**, 3433–3458.
13. H. H. Wang, L. Xue, C. L. Yu, Y. Y. Qian, H. Jiang, *Dyes Pigm.*, 2011, **91**, 350–355.
14. E. Coronado, J. R. G. Mascaros, C. M. Gastaldo, E. Palomares, J. R. Durrant, R. Vilar, M. Gratzel, M. K. Nazeeruddin, *J. Am. Chem. Soc.*, 2005, **127**, 12351–12356.
15. E. M. Nolan, S. J. Lippard, *J. Am. Chem. Soc.*, 2007, **129**, 5910–5918.
16. Z. Dong, X. Tian, Y. Chen, J. Hou, Y. Guo, J. Sun, J. Ma, *Dyes Pigm.*, 2013, **97**, 324–329.
17. J. Liu, D. Wu, C. Duan, Y. Guan, *Talanta*, 2013, **105**, 87–92.
18. J. Nia, Q. Li, B. Li, L. Zhang, *Sens. Actuators, B*, 2013, **186**, 278–285.
19. X. Chen, S. W. Nam, M. J. Jou, Y. Kim, S. J. Kim, S. Park, J. Yoon, *Org. Lett.*, 2008, **10**, 5235–5238.
20. Q. Li, M. Peng, H. Li, C. Zhong, L. Zhang, X. Cheng, X. Peng, Q. Wang, J. Qin, Z. Li, *Org. Lett.*, 2012, **14**, 2094–2097.
21. M. Kumar, A. Dhir, V. Bhalla, R. Sharma, R. K. Puri, R. K. Mahajan, *Analyst*, 2010, **135**, 1600–1605.
22. Y. Yan, Z. Che, X. Yu, X. Zhi, J. Wang, H. Xu, *Bioorg. Med. Chem.*, 2013, **21**, 508–513.
23. L. E. S. Figueroa, M. E. Moragues, E. Climent, A. Agostini, R. M. Manez, F. Sancenon, *Chem. Soc. Rev.*, 2013, **42**, 3489–3613.
24. Y. Yang, Q. Zhao, W. Feng, F. Li, *Chem. Rev.*, 2013, **113**, 192–270.
25. M. Formica, V. Fusi, L. Giorgi, M. Micheloni, *Coord. Chem. Rev.*, 2012, **256**, 170–192.
26. J. Wu, W. Liu, J. Ge, H. Zhang, P. Wang, *Chem. Soc. Rev.*, 2011, **40**, 3483–3495.
27. D. T. Quang, J. S. Kim, *Chem. Rev.*, 2010, **110**, 6280–6301.
28. X. Chen, T. Pradhan, F. Wang, J. S. Kim, J. Yoon, *Chem. Rev.*, 2012, **112**, 1910–1956.
29. H. N. Kim, M. H. Lee, H. J. Kim, J. S. Kim, *Chem. Soc. Rev.*, 2008, **37**, 1465–1472.
30. F. Yan, D. Cao, N. Yang, Q. Yu, M. Wang, L. Chen, *Sens. Actuators, B*, 2012, **162**, 313–320.
31. B. C. Yin, M. You, W. Tan, B. C. Ye, *Chem. Eur. J.*, 2012, **18**, 1286–1289.
32. X. Wang, P. Wang, Z. Dong, Z. Ma, J. Jiang, R. Li, J. Ma, *Nanoscale Res Lett.*, 2010, **5**, 1468–1473.
33. Y. Chen, Z. H. Sun, B. E. Song, Y. Liu, *Org. Biomol. Chem.*, 2011, **9**, 5530–5534.
34. C. Chen, R. Wang, L. Guo, N. Fu, H. Dong, Y. Yuan, *Org. Lett.*, 2011, **13**, 1162–1165.
35. M. Suresh, A. K. Mandal, S. Saha, E. Suresh, A. Mandoli, R. D. Liddo, P. P. Parnigotto, A. Das, *Org. Lett.*, 2010, **12**, 5406–5409.
36. R. R. Avirah, K. Jyothish, D. Ramaiah, *Org. Lett.*, 2007, **9**, 121–124.
37. S. K. Ko, Y. K. Yang, J. Tae, I. Shin, *J. Am. Chem. Soc.*, 2006, **128**, 14150–14155.
38. Y. Zhao, B. Zheng, J. Du, D. Xiao, L. Yang, *Talanta*, 2011, **85**, 2194–2201.
39. Z. Wu, X. Wu, Y. Yang, T. B. Wen, S. Han, *Bioorg. Med. Chem. Lett.*, 2012, **22**, 6358–6361.
40. X. Chen, S. Wu, J. Han, S. Han, *Bioorg. Med. Chem. Lett.*, 2013, **23**, 5295–5299.
41. Z. Wu, X. Wu, Z. Li, Y. Yang, J. Han, S. Han, *Bioorg. Med. Chem. Lett.*, 2013, **23**, 4354–4357.
42. A. Chatterjee, M. Santra, N. Won, S. Kim, J. K. Kim, S. B. Kim, K. H. Ahn, *J. Am. Chem. Soc.*, 2009, **131**, 2040–2041.
43. S. Park, W. Kim, K. M. K. Swamy, H. Y. Lee, J. Y. Jung, G. Kim, Y. Kim, S. J. Kim, J. Yoon, *Dyes Pigm.*, 2013, **99**, 323–328.
44. H. E. Kaoutit, P. Estevez, S. Ibeas, F. C. Garcia, F. Serna, F. B. Benabdelouahab, J. M. Garcia, *Dyes Pigm.*, 2013, **96**, 414–423.
45. W. Liu, J. Chen, L. Xu, J. Wu, H. Xu, H. Zhang, P. Wang, *Spectrochim. Acta, Part A*, 2012, **85**, 38–42.
46. J. Q. Li, T. B. Wei, Q. Lin, P. Li, Y. M. Zhang, *Spectrochim. Acta, Part A*, 2011, **83**, 187–193.
47. K. Liu, Y. Zhou, C. Yao, *Inorg Chem Commun.*, 2011, **14**, 1798–1801.
48. F. Song, S. Watanabe, P. E. Floreancig, K. Koide, *J. Am. Chem. Soc.*, 2008, **130**, 16460–16461.
49. Y. K. Yang, K. J. Yook, J. Tae, *J. Am. Chem. Soc.*, 2005, **127**, 16760–16761.
50. L. E. Page, X. Zhang, A. M. Jawaid, P. T. Snee, *Chem. Commun.*, 2011, **47**, 7773–7775.
51. N. I. Georgiev, A. R. Sakr, V. B. Bojinov, *Dyes Pigm.*, 2011, **91**, 332–339.
52. K. Lang, J. W. Chin, *Nat Chem*, 2013, **5**, 81–82.
53. W. Lin, D. Buccella, S. J. Lippard, *J. Am. Chem. Soc.*, 2013, **135**, 13512–13520.
54. T. Guo, L. Cui, J. Shen, R. Wang, W. Zhu, Y. Xu, X. Qian, *Chem. Commun.*, 2013, **49**, 1862–1864.
55. L. Xue, C. Liu, H. Jiang, *Chem. Commun.*, 2009, **9**, 1061–1063.
56. M. Savarese, A. Aliberti, I. D. Santo, E. Battista, F. Causa, P. A. Netti, N. Rega, *J. Phys. Chem.* 2012, **116**, 7491–7497.
57. J. N. Demas, G. A. Crosby, *J. Phys. Chem.* 1971, **75**, 991–1024.
58. F. Yan, D. Cao, N. Yang, M. Wang, L. Dai, C. Li, L. Chen, *Spectrochim. Acta, Part A*, 2013, **106**, 19–24.
59. S. Hussain, D. A. Rodgers, H. M. Duhart, S. F. Ali, *J. Environ. Sci. Health B*, 1998, **32**, 395–409.
60. K. M. Madsen, *Kidney Int.*, 1980, **18**, 445–453.
61. C. C. Bridges, R. K. Zalups, *Toxicol Appl Pharm.*, 2005, **204**, 274–308.
62. M. H. Hazelhoff, R. P. Bulacio, A. M. Torres, *Int. J. Mol. Sci.*, 2012, **13**, 10523–10536.
63. S. Omata, M. Sato, K. Sakimura, H. Sugano, *Arch. Toxicol.*, 1980, **44**, 231–241.
64. R. K. Zalups, *Toxicol Appl Pharm.*, 1998, **151**, 192–199.
65. F. J. Dieguez-Acuna, W. W. Polk, M. E. Ellis, P. L. Simmonds, J. V. Kushleika, J. S. Woods, *Toxicol. Sci.*, 2004, **82**, 114–123.